Chemical Engineering Journal 147 (2009) 79–86

Contents lists available at ScienceDirect

Chemical Engineering Journal

journal homepage: www.elsevier.com/locate/cej

Surface morphology, crystal structure and orientation of aluminium coatings electrodeposited on mild steel in ionic liquid

Guikuan Yue[a,b], Xingmei Lu[a], Yanli Zhu[a], Xiangping Zhang[a], Suojiang Zhang[a,*]

[a] Institute of Process Engineering, Chinese Academy of Sciences, Beijing 100190, PR China
[b] Graduate University of Chinese Academy of Sciences, Beijing 100049, PR China

ARTICLE INFO

Keywords:
Ionic liquid
Aluminium
Surface morphology
Orientation
Electrodeposition

ABSTRACT

Galvano-static electrodeposition was used to electrodeposit aluminium on mild steel in $AlCl_3$/[bmim]Cl (1-butyl-3-methylimidazolium chloride) ionic liquid at variable temperatures (308–328 K). Effects of variations in current density and temperature on surface morphology and crystal orientations were systematically studied. Results show current density certainly caused changes in the morphology and deposit microstructure, and the type of deposit microstructure changed rapidly as a function of temperature, especially at higher current density. It was indicated that all of the electrodeposits exhibited a strong preferred (2 0 0) crystallographic orientation. Compared with the (2 0 0) reflection, the preferred (2 2 2) orientation was relatively weak for most samples, and under higher temperature and current density it disappears. The (1 1 1), (2 2 0), and (3 1 1) reflections were relatively weak.

1. Introduction

Interest in the preparation of aluminium coatings has steadily increased due to its excellent corrosion resistance, decorativeness and physicochemical properties. Several procedures can be employed for coating of Al on various substrates—mainly on steels—such as hot dipping [1,2], thermal spraying [3], sputter deposition [4,5], vapor deposition [6,7], etc. These techniques are rather expensive and often impractical, and the main disadvantages of them are the uneven surfaces, impossibility of controlling the thickness and quality of the layer, and possible damage of the specimen at employed high temperatures. On the contrary, the electrodeposition method is a valuable technology due to its advantages such as mild conditions, easy operation, uniform thickness distribution, adjustable microstructure of the deposited layers and unlimited substrates (including arbitrary shapes or complex geometries).

Electrodeposition of Al from aqueous solutions is impossible owing to a massive hydrogen evolution at the cathode caused by the rather negative standard potential of Al/Al(III) couple (−1.67 V vs. NHE). Essentially, two types of aprotic electrolytes are eligible: organic solvents and molten salts. There are three typical kinds of organic solvents used for electrodeposition of Al: aromatic hydrocarbons [8,9], dimethylsulfone [10,11] and ethers [12,13]. At present, only two commercial processes based on organic solvents are available for electroplating of Al: SIGAL [8] and REAl [14,15]. The main disadvantages of such processes are the flammability and volatility of the electrolytes. High temperature inorganic molten salts, such as NaCl–KCl [16], $AlCl_3$–NaCl [17] and $AlCl_3$–NaCl–KCl [18] have been extensively studied for the electrodeposition of Al. However, the high temperature and their highly corrosive natures bring great difficulties for finding container materials that can withstand chemical attack by the melts.

Over the last decades, aluminium plating in the room temperature molten salts (also called room temperature ionic liquids—RTILs), has received considerable attention. As a new and novel generation of solvents, RTILs exhibit many attractive properties, including excellent chemical and thermal stability, low melting points with negligible vapor pressure, high electrical conductivity and solvent transport properties, wide range of operational liquid temperature, ability to dissolve various organic, inorganic, and organometallic compounds and large electrochemical window of about 4.0 V. These properties give RTILs a certain potential to play a vital role in the electrochemistry field. Electrodeposition of Al from $AlCl_3$ based ILs were intensively and systematically studied from the 1980s, seeing for example [19–26]. These ILs exhibit adjustable Lewis acidity depending on the molar ratio of $AlCl_3$/IL [27]. Electrodeposition of Al can only be performed under the Lewis acidic condition, in which the $Al_2Cl_7^-$ precursor, the dominant species in the electrolyte, can be electrochemically reduced to the metallic form according to the following reaction [28]:

$$4Al_2Cl_7^- + 3e^- \rightarrow Al + 7AlCl_4^- \quad (1)$$

A lot of progresses have been made and the electrodeposition was performed on various substrates such as platinum [20,29], tungsten

* Corresponding author. Tel.: +86 10 8262 7080; fax: +86 10 8262 7080.
E-mail address: sjzhang@home.ipe.ac.cn (S. Zhang).

1385-8947/$ – see front matter © 2008 Elsevier B.V. All rights reserved.
doi:10.1016/j.cej.2008.11.044

[20,21], gold [30,31], copper [32,33], glass carbon [20] and mild steel [34]. However, little information has been reported in the literature about the systematic study of the relationships between deposit appearance, surface morphology and current efficiency with current density and temperature, respectively. Moreover, there is a lack of published reports describing the effects of current density and temperature on the crystal structure and orientation of Al electrodeposited from RTILs. In this work, we describe comprehensive and detailed investigation of surface morphology and crystal orientation of Al coatings electroplated on mild steel substrates in Lewis acidic $AlCl_3$/[bmim]Cl ILs by galvano-static technique. Temperatures were determined in the range from 308 K to 328 K based on our parallel study, where smoother, denser and brighter deposits were obtained.

2. Experimental

The electrolyte preparation and subsequent eletrodeposition were both conducted in an electrolytic cell with a jacket under a dry nitrogen atmosphere. [bmim]Cl was synthesized in our laboratory. Anhydrous $AlCl_3$ (powder) obtained from Beijing Chemical Reagents Company, without further purification, was used as the initial source of Al. The Lewis acidic electrolyte (with 2.0:1 molar ratio of $AlCl_3$/[bmim]Cl) was carefully prepared by mixing precise quantities of $AlCl_3$ and [bmim]Cl. The obtained electrolyte was continuously stirred for several hours to ensure uniformity. Moreover, the electrolyte was used without further purification so that the electrodeposition of Al could be investigated in the conditions easily transferable to the industry.

All the experiments were conducted using a three-electrode system: Al plate (Beijing Chemical Reagents Company, $\geq$99.0%), mild steel plate and ultra-pure Al wire (Beijing Mountain Technical Development Center for Non-Ferrous Metals, 99.999%) were used as counter electrode, working electrode, and reference electrode, respectively. The distance between the cathode and the anode was ca. 2.0 cm. Al plate was dipped in NaOH, rinsed with deionized water, followed by acetone and then dried before use; mild steel was immerged in boiling NaOH, dipped in 20–30% HCl (by volume), washed with deionized water and finally dried. Prior to use, the working electrodes were mechanically polished with sand paper, treated with a dilute mixture of hydrochloric acid (37%) and sulfuric acid (98%), rinsed with deionized water, and finally immersed into dichloromethane for degreasing. After completing the pretreatments, the electrodes were assembled for immediate use. The depositions were carried out under a predetermined experimental temperature for 0.5 h with a constant stirring speed. Following each deposition experiment, excess IL was removed from the sample by washing in absolute alcohol; then the sample was rinsed with deionized water and dried with cool air.

Electrochemical measurements were performed using a CHI660C Electrochemical Workstation controlled with a personal computer. Surface morphology of the films was examined with emission scanning electron microscope (SEM, JSM-6700F). The compositional analysis of the deposits was confirmed by energy dispersive analysis by X-ray (EDAX, Oxford INCA300). The crystal structure was studied on a X' Pert PRO (PANalytical) X-ray diffractometer with Cu Kα radiation.

3. Results and discussion

3.1. Effect of current density on the surface morphology

Current density usually has an important effect on the deposit brightness, thickness distribution, current efficiency and microstructure of the electrodeposits. Herein the effect of current density was investigated from 8 mA/cm^2 to 24 mA/cm^2 at 308 K, from 8 mA/cm^2 to 26 mA/cm^2 at 318 K and from 8 mA/cm^2 to 32 mA/cm^2 at 328 K in 2.0:1 $AlCl_3$/[bmim]Cl for 0.5 h in galvanostatic mode (the supreme current density is enhanced with the temperature increasing). All of the Al-deposited samples were dense, adherent and homogeneous and the surface coverage was quite satisfactory.

At 308 K, the deposits formed at 12–24 mA/cm^2 are quite smooth and bright, and thus the optimum current densities were determined in this range. The current efficiency decreases with increase in the current density in the range of 96.1–78.5%. The current efficiency decreases to be ca. 78.5% at 24 mA/cm^2. As the current density increases the total charge though the cell increases, hence the theoretical amount deposited also increases. However, the actual weight deposited does not follow a similar trend as that of current density due to the current loss (polarization effects) involved in electrolysis process. Therefore, lower current efficiencies can be attributed to the above phenomena. The surface morphologies of the Al-coated mild steel substrates were further examined by SEM. Fig. 1 shows the SEM micrographs of the deposits obtained in 2.0:1 $AlCl_3$/[bmim]Cl at 308 K for 0.5 h as a function of the current density (from 12 mA/cm^2 to 24 mA/cm^2). The deposits obtained at 12 mA/cm^2, 16 mA/cm^2 and 20 mA/cm^2 display similar microstructures (Fig. 1a–c) and the deposited layer appeared quite dense and uniformly covered the entire mild steel substrate. Relatively scattered surface with smaller clusters of particles is observed on the deposits obtained at 24 mA/cm^2 (Fig. 1d). From the SEM analysis of the deposit microstructure at 308 K, it appears that the morphology of deposits was relatively independent of current density.

However, deposit microstructure obtained at higher temperature (318 K) of the electrolyte revealed interesting features as a function of current density. Fig. 2 shows the SEM micrographs of Al coatings with a current density of 12–24 mA/cm^2 at 318 K. The deposits obtained at 12 mA/cm^2 display continuous and dense microstructure with some nodules (Fig. 2a). At higher current densities a compact layer of deposit microstructure with spherical particles was observed as seen in Fig. 2b and c, except that the latter (Fig. 2c) is much denser and more homogeneous with smaller particles. With the highest current density in Fig. 2d the deposit morphology reveals a dense and compact layer containing non-spherical particles formed as small clusters. It can be seen from the above microstructures that at 318 K, the type of deposit microstructure changed obviously as a function of current density. Unlike the case of low temperature (308 K) where the deposit microstructure is relatively independent of current density, at 318 K, the influence of current density is clearly seen on the deposit microstructure. The influence of increased temperature seems to lead to a nucleation-controlled microstructure. Current efficiencies decrease with increase in the current density in the range of 94.8–80.6%. Compared with the one gained at 308 K, the relationship between the current efficiency and current density at 318 K seems to be the same as that of 308 K.

Fig. 3 shows the SEM images of the deposits obtained in 2.0:1 $AlCl_3$/[bmim]Cl for 0.5 h with various current densities at much higher temperature (328 K). In Fig. 3a, deposits with homogeneous spherical particles in an average size of 10 μm can be observed where some amount of agglomeration of particles appears to have taken place. In Fig. 3b, the deposit morphology reveals a non-continuous layer containing squama particles formed as small clusters with an average size of 8 μm. At higher current densities a compact layer of deposit microstructure with spiculate particles was observed as seen in Fig. 3c and d, except that particles in Fig. 3d are a little smaller, more homogeneous and much denser than those in Fig. 3c. It can be seen from the above microstructures that at 328 K, the type of deposit microstructure also changed apparently

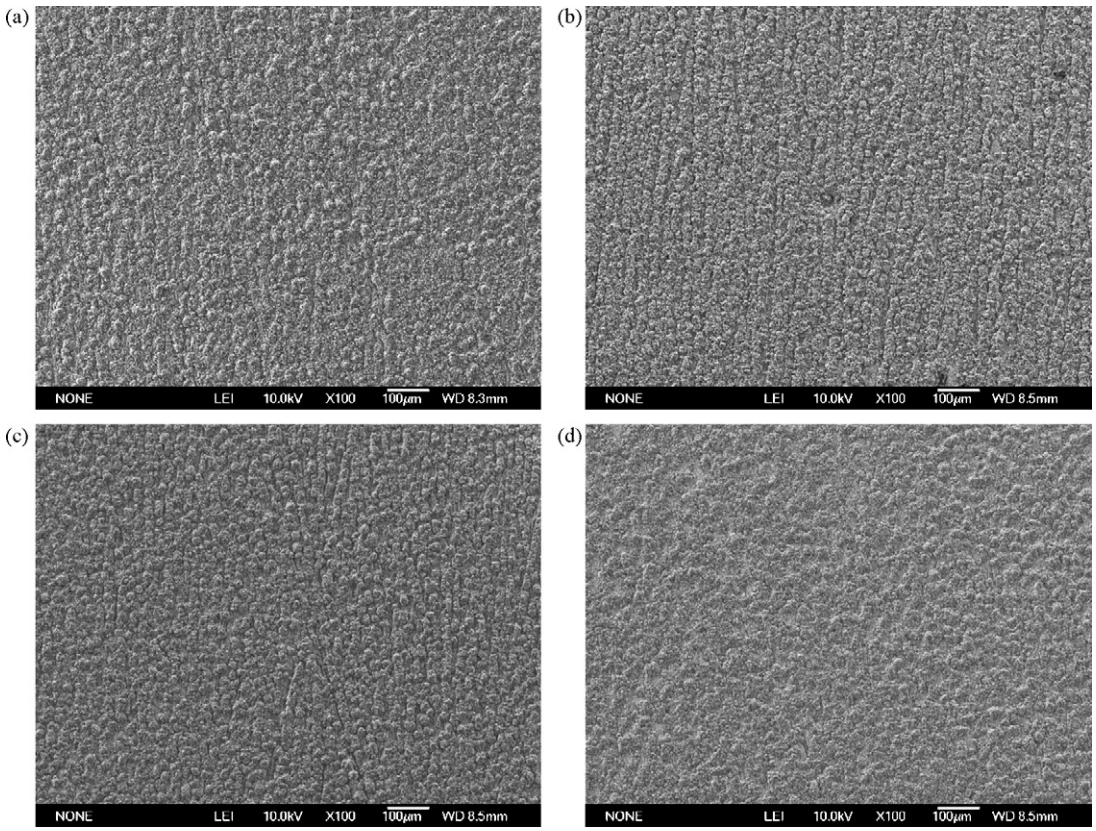

Fig. 1. SEM micrographs of the aluminium coatings obtained from 2.0:1 $AlCl_3$/[bmim]Cl at 308 K for 0.5 h under stirring condition by magnetic stirrer (300 rpm) with different current densities (mA/cm^2): (a) 12; (b) 16; (c) 20; (d) 24. Their nominal thicknesses are 7.16 μm, 9.19 μm, 11.08 μm and 11.68 μm, respectively.

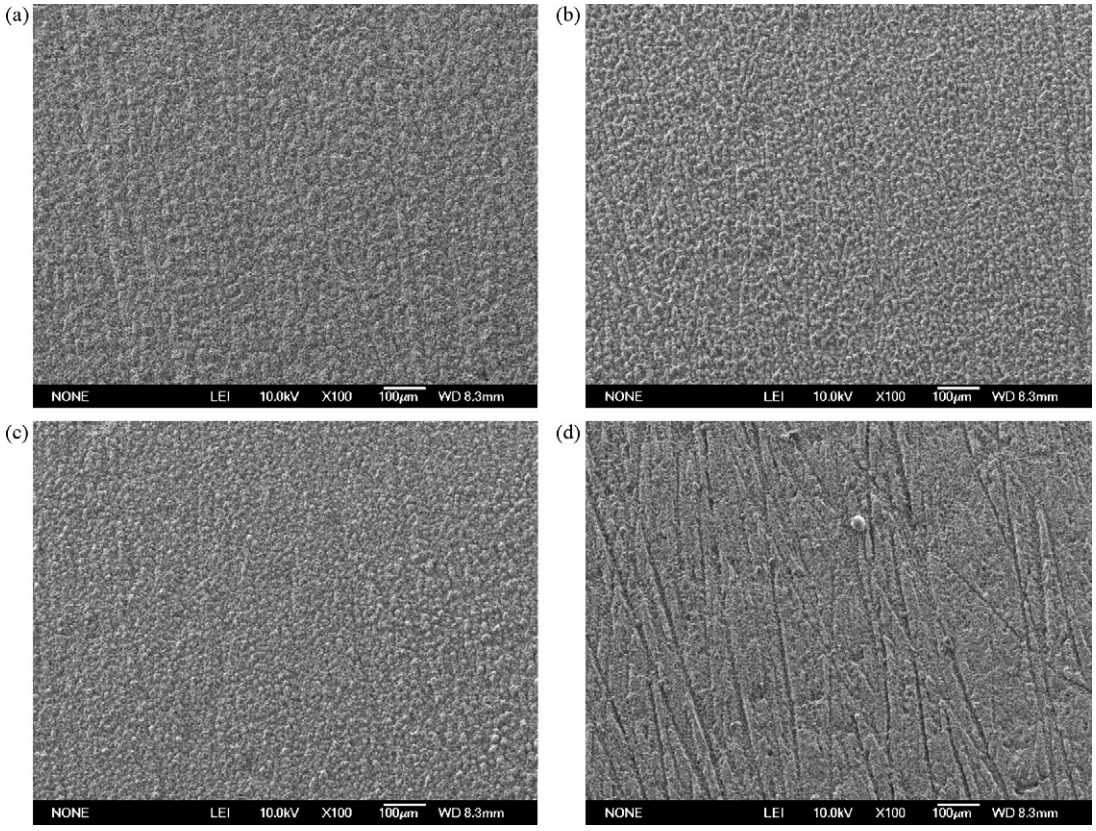

Fig. 2. SEM micrographs of the aluminium coatings obtained from 2.0:1 $AlCl_3$/[bmim]Cl at 318 K for 0.5 h under stirring condition by magnetic stirrer (300 rpm) with different current densities (mA/cm^2): (a) 12; (b) 16; (c) 20; (d) 24. Their nominal thicknesses are 7.07 μm, 9.05 μm, 10.73 μm and 13.53 μm, respectively.

as a function of current density. The color of gained Al coatings in 2.0:1 $AlCl_3$/[bmim]Cl at 348 K for 0.5 h were darker than ones obtained at 308 K and 318 K in general. At 328 K, with the increase of current density, the color gradually changed to darker grey. The current efficiencies decrease with increase in the current density in the range of 93.3–72.2%. Compared with the ones gained at 308 K and 318 K, similar relationship between the current efficiency and current density was obtained.

From the above analysis, it can be seen that current density certainly caused changes in the morphology and deposit microstructure: at 308 K, it appears that the morphology of deposits was relatively independent of current density; at 318 K and 328 K, the type of deposit microstructure changed obviously as a function of current density.

3.2. Effect of temperature on the surface morphology

The effect of temperature on the surface morphology was investigated in 2.0:1 $AlCl_3$/[bmim]Cl under different current densities—12 mA/cm^2, 20 mA/cm^2 and 24 mA/cm^2. It was found that at 12 mA/cm^2, the deposits obtained at 308 K and 318 K display continuous and dense microstructure with some nodules (Figs. 1a and 2a), and deposits with homogeneous spherical particles can be observed at 328 K (Fig. 3a), which shows that the morphology of deposits was relatively independent of current density.

The deposits obtained at 20 mA/cm^2 with a temperature increasing from 308 K to 328 K display different results (Figs. 1c, 2c and 3b). At 308 K, the deposit display relatively rough surface with some nodules. Deposits obtained at 318 K are a compact layer of microstructure with spherical particles. A non-continuous layer containing squama particles formed as small clusters was observed at 328 K as seen in Fig. 3b. It can be seen from the above microstructures that at 20 mA/cm^2, the type of deposit microstructure changed rapidly as a function of temperature.

Deposit microstructures obtained at higher current density (24 mA/cm^2) with different temperatures are also quite different from those at lower current density (12 mA/cm^2). The deposits obtained at 308 K (Fig. 1d) shows relatively scattered surface with small clusters of particles. A dense and compact layer containing non-spherical particles formed as small clusters at 318 K is shown in Fig. 2d. At 328 K a compact layer of deposit microstructure with spiculate particles was observed in Fig. 3c.

From the analysis of the deposit microstructure under different current densities, it appears that the type of deposit microstructure changed rapidly as a function of temperature and the morphology of deposits was greatly dependent of temperature, especially at higher current density. The combined influence of increased temperature and current density seems to have resulted in a nucleation-controlled microstructure.

3.3. Effect of current density on the crystal structure and orientation of aluminium coatings

The chemical compositions of the samples electrodeposited under different conditions were inspected with an EDAX and the results revealed an identical spectrum. Fig. 4 shows the EDAX analyses of the deposits obtained on the working electrodes after 0.5 h in 2.0:1 $AlCl_3$/[bmim]Cl at 318 K and 20 mA/cm^2. As expected, the deposits display a strong peak for aluminium, and slight peaks of iron and oxygen. The Fe detected in the Al deposits may come from the substrate and the detected O may result from the oxidation of Al or Fe. Table 1 shows the components of the deposits

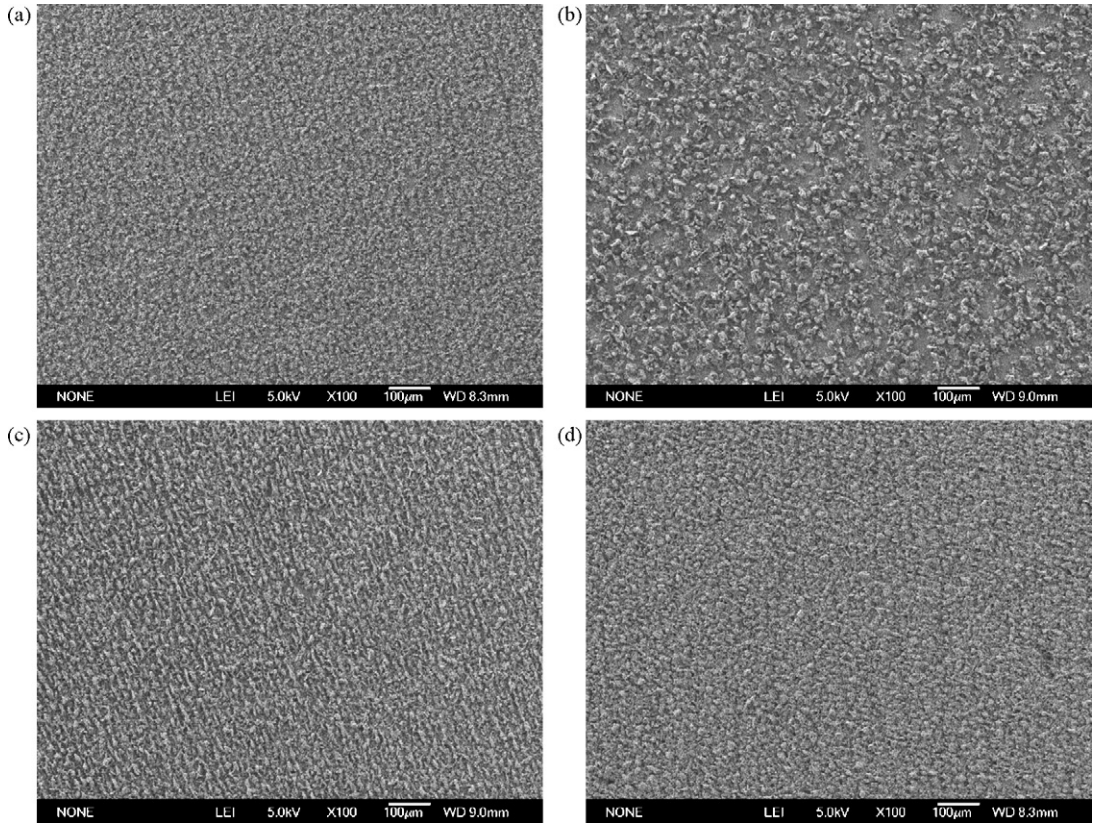

Fig. 3. SEM micrographs of the aluminium coatings obtained from 2.0:1 $AlCl_3$/[bmim]Cl at 328 K for 0.5 h under stirring condition by magnetic stirrer (300 rpm) with different current densities (mA/cm^2): (a) 12; (b) 20; (c) 24; (d) 32. Their nominal thicknesses are 6.96 μm, 10.50 μm, 11.21 μm and 14.35 μm, respectively.

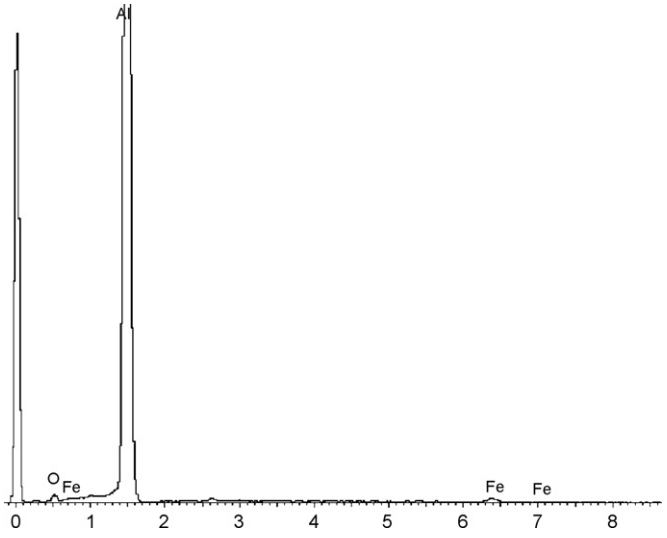

Fig. 4. EDAX spectra of the deposit on cathode in 2.0:1 $AlCl_3$/[bmim]Cl for 0.5 h at 318 K and 20 mA/cm^2.

Table 1
Components of the deposit in 2:1 $AlCl_3$/[bmim]Cl for 0.5 h at 318 K and 20 mA/cm^2.

Element	Weight%	Atomic%
O K	2.05	3.43
Al K	96.85	96.04
Fe K	1.10	0.53
Totals	100.00	

clearly.

Crystal structure analyses were also carried out using XRD, and the acquired diffraction patterns of the obtained samples show only patterns of aluminium metal (Fig. 5). The diffraction peaks attributed to pure Al with a face-centered cubic structure (fcc) were clearly detected from both of the samples. Similar results are observed for other samples. The only difference from the JCPDS card is the ratio of peak intensities which will be discussed in the following.

The influence of bath conditions, such as bath composition, current density and temperature on the preferred orientation of almost every metal that can be electrodeposited has been widely studied. A general review was given by Pangarov [35]. The orientation of the obtained samples was studied by analyzing the results of XRD [36–38]. The normalized integrated intensity, P_{hkl}, for the (1 1 1), (2 0 0), (2 2 0), (3 1 1) and (2 2 2) reflections was calculated by using the following expression:

$$P_{hkl} = \frac{I_{hkl}/\sum I_{hkl}}{Ir_{hkl}/\sum Ir_{hkl}} \quad (2)$$

where I_{hkl} is the peak intensity of the (hkl) reflection for the obtained samples; $\sum I_{hkl}$ is the sum of peak intensities for the obtained samples; Ir_{hkl} is the peak intensity of the (hkl) reflection for the JCPDS card no. 01-089-2769 and $\sum Ir_{hkl}$ is the sum of peak intensities for the JCPDS card no. 01-089-2769.

The calculated results of the effects of current density on the preferred orientation under different temperatures are plotted in Figs. 6–8. It is shown in Fig. 6 that all of the electrodeposits at 308 K with different current densities exhibited a preferred (2 0 0) and (2 2 2) crystallographic orientation and the strongest orientation of (2 0 0) is observed at 16 mA/cm^2. The (2 0 0) intensity first increases, and then decreases; in contrast, the (2 2 2) intensity decreases first, and then increases; the (1 1 1), (2 2 0), and (3 1 1) reflections are relatively weak. Crystallographic orientations of electrodeposits obtained at 318 K with different current densities in Fig. 7 show that there appears to be a similar impact of current density on the crystallographic orientation compared with that at 308 K, except that the strongest orientation of (2 0 0) is observed at higher current density (20 mA/cm^2).

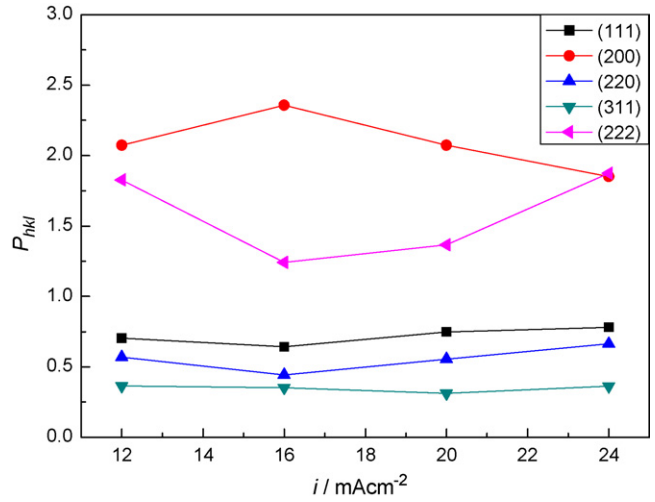

Fig. 6. Normalized peak intensity, P_{hkl}, from XRD reflections of the samples obtained with different current densities in 2.0:1 $AlCl_3$/[bmim]Cl for 0.5 h at 308 K.

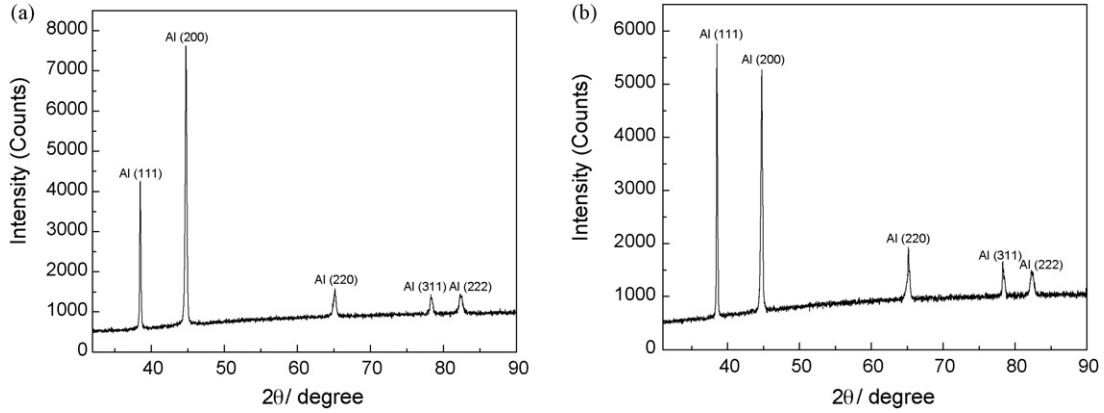

Fig. 5. XRD pattern of electro-deposit Al on the mild steel at galvano-static conditions (mild steel plate as working electrode; Al plate as counter electrode; Al-wire as reference electrode; concentration ratio, 2.0:1 and time, 0.5 h): (a) at 318 K and 20 mA/cm^2; (b) at 328 K and 24 mA/cm^2.

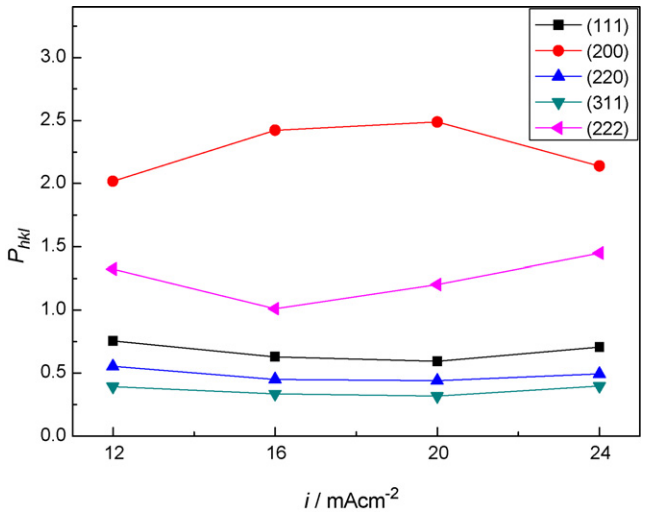

Fig. 7. Normalized peak intensity, P_{hkl}, from XRD reflections of the samples obtained with different current densities in 2.0:1 $AlCl_3$/[bmim]Cl for 0.5 h at 318 K.

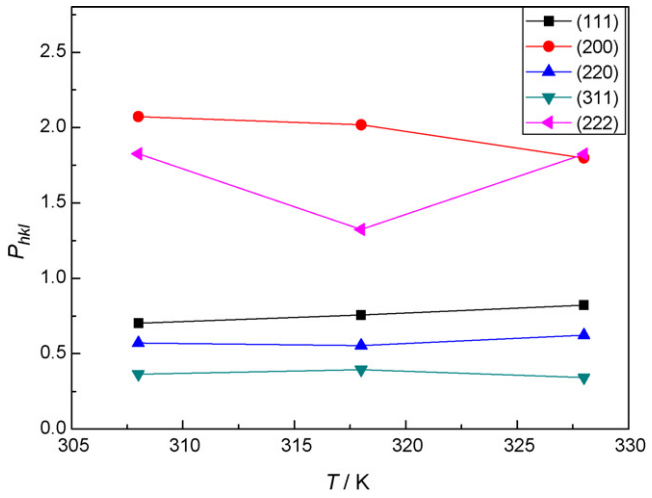

Fig. 9. Normalized peak intensity, P_{hkl}, from XRD reflections of the samples obtained with a current density of 12 mA/cm^2 in 2.0:1 $AlCl_3$/[bmim]Cl for 0.5 h as a function of temperature.

However, at higher temperature (328 K), crystallographic orientations of electrodeposits revealed quite different features as a function of current density (in Fig. 8). The (2 0 0) intensity increases along with the current density in general and the (2 2 2) intensity decreases, though some slight increase in the (2 0 0) and decrease in the (2 2 2) intensities were observed. Under lower current density ($\leq$16 mA/cm^2), the electrodeposits exhibited a preferred (2 0 0) and (2 2 2) crystallographic orientation and the intensities of (2 0 0) and (2 2 2) are equal to each other at 12 mA/cm^2. As the current density increases ($\geq$20 mA/cm^2), only preferred (2 0 0) orientation was observed and the (2 2 2) reflection was essentially equal to that of a randomly referenced oriented sample. The (1 1 1), (2 2 0), and (3 1 1) reflections were relatively weak.

Based on the above analysis, it can be concluded that crystallographic orientations of electrodeposits revealed quite different features as a function of current density along with the increased temperature: at lower temperature (308 K and 318 K), a preferred (2 0 0) and (2 2 2) crystallographic orientation was observed and the (2 0 0) and (2 2 2) intensities vary according to similar rules, except that the strongest orientation of (2 0 0) is observed at higher current density at 318 K; at higher temperature (328 K), under lower current density ($\leq$16 mA/cm^2), the electrodeposits exhibited a preferred (2 0 0) and (2 2 2) crystallographic orientation and as the current density is increased ($\geq$20 mA/cm^2), only preferred (2 0 0) orientation was observed.

3.4. Effect of temperature on the orientation of aluminium coatings

According to the above method for analyzing the crystallographic orientations of electrodeposits, the calculated results of the effects of temperature on the preferred orientation under different current densities are plotted in Figs. 9–12.

It is shown in Fig. 9 that all of the electrodeposits at different temperatures with a current density of 12 mA/cm^2 exhibited a preferred (2 0 0) and (2 2 2) crystallographic orientation. The (2 0 0) intensity decreases with the temperature increasing from 308 K to 328 K; the (2 2 2) intensity decreases first, then increases and was equal to (2 0 0) at 328 K; the (1 1 1), (2 2 0), and (3 1 1) reflections were relatively weak and the intensities increase along with temperature.

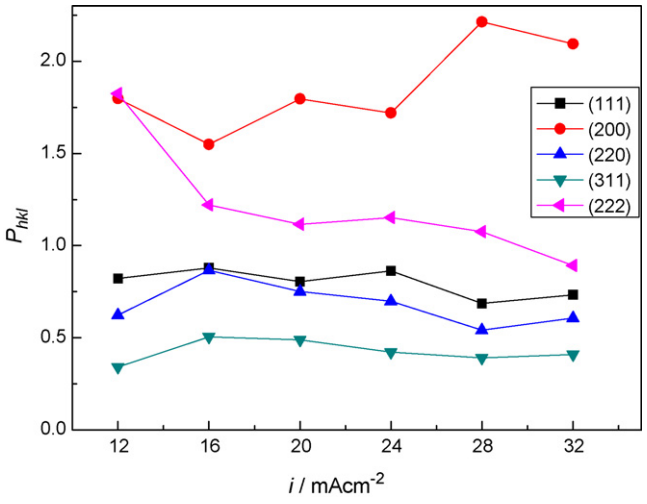

Fig. 8. Normalized peak intensity, P_{hkl}, from XRD reflections of the samples obtained with different current densities in 2.0:1 $AlCl_3$/[bmim]Cl for 0.5 h at 328 K.

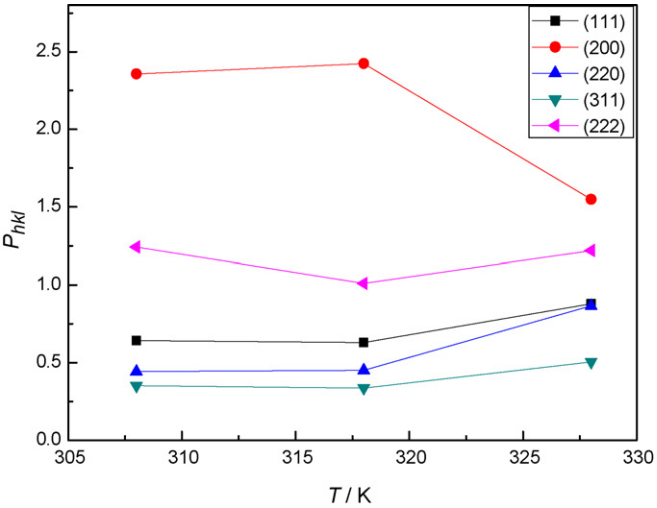

Fig. 10. Normalized peak intensity, P_{hkl}, from XRD reflections of the samples obtained with a current density of 16 mA/cm^2 in 2.0:1 $AlCl_3$/[bmim]Cl for 0.5 h as a function of temperature.

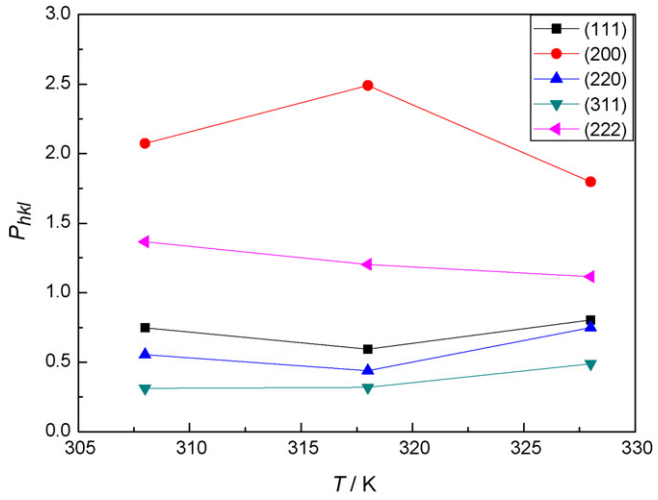

Fig. 11. Normalized peak intensity, P_{hkl}, from XRD reflections of the samples obtained with a current density of 20 mA/cm^2 in 2.0:1 $AlCl_3$/[bmim]Cl for 0.5 h as a function of temperature.

However, under higher current density (16 mA/cm^2), the electrodeposits exhibited a preferred (2 0 0) crystallographic orientation and the strongest orientation of (2 0 0) is observed at 318 K (Fig. 10). The (2 2 2) intensity decreases first and then increase with the temperature: under lower temperature (308 K) and higher temperature (328 K), a preferred (2 2 2) crystallographic orientation could be observed; at 318 K, the (2 2 2) intensity was essentially equal to that of a randomly referenced oriented sample. The (1 1 1), (2 2 0), and (3 1 1) reflections were relatively weak and the intensities increase first and then decrease along with increased temperature. Similar results were obtained under higher current density (20 mA/cm^2), and the only difference is that the (2 2 2) intensity decreases along with the temperature (Fig. 11).

Crystallographic orientations of electrodeposits obtained at different temperatures with a current density of 24 mA/cm^2 in Fig. 12 show that similar results of the influences of temperature on the crystallographic orientation were obtained compared to those under 20 mA/cm^2, except that at lower temperature (308 K) the (2 2 2) intensity was equal to that of (2 0 0).

From the above analyses, conclusions can be drawn that in general the (2 0 0) and (2 2 2) intensities decrease, and the (1 1 1), (2 2 0), and (3 1 1) intensities increase. Under lower current density (12 mA/cm^2 and 16 mA/cm^2) a preferred (2 0 0) and (2 2 2) crystallographic orientation could be obtained; however, under higher current densities (20 mA/cm^2 and 24 mA/cm^2), the preferred (2 2 2) crystallographic orientation becomes lower quickly with increased temperature and disappears at 328 K.

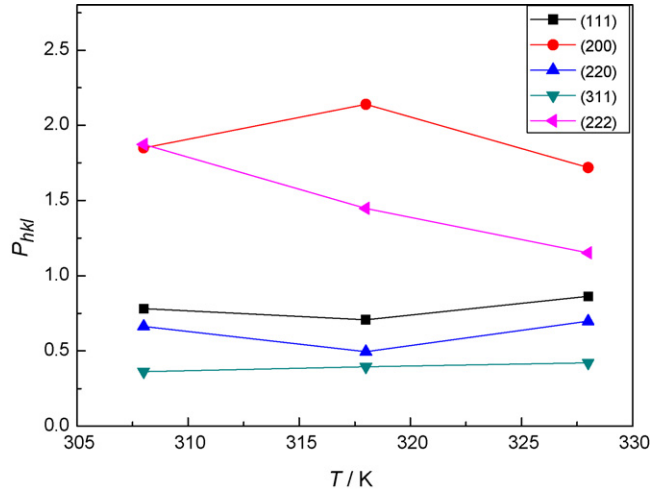

Fig. 12. Normalized peak intensity, P_{hkl}, from XRD reflections of the samples obtained with a current density of 24 mA/cm^2 in 2.0:1 $AlCl_3$/[bmim]Cl for 0.5 h as a function of temperature.

4. Conclusions

It can be concluded that surface morphology and crystal orientation of aluminium deposits on mild steel substrates from Lewis acidic $AlCl_3$/[bmim]Cl ILs are affected markedly by variations in current density and temperature. It appears that the morphology of deposits under lower temperature (308 K) was relatively independent of current density. Deposit microstructure obtained at higher temperature (318 K and 328 K) revealed obvious changes as a function of current density. It was shown that the type of deposit microstructure changed apparently as a function of temperature and the morphology of deposits was greatly dependent of temperature, especially at higher current density. At lower temperature (308 K and 318 K), with increased current density, a preferred (2 0 0) and (2 2 2) crystallographic orientation was observed and the (2 0 0) and (2 2 2) intensities vary according to similar rules; at higher temperature (328 K), under lower current density ($\leq$16 mA/cm^2), the electrodeposits exhibited a preferred (2 0 0) and (2 2 2) crystallographic orientation and as the current density is increased ($\geq$20 mA/cm^2), only preferred (2 0 0) orientation was observed. It was indicated that as temperature was increased, under lower current density (12 mA/cm^2 and 16 mA/cm^2) a preferred (2 0 0) and (2 2 2) crystallographic orientation can be obtained; however, under higher current densities (20 mA/cm^2 and 24 mA/cm^2), the preferred (2 0 0) and (2 2 2) crystallographic orientation became lower quickly and the preferred (2 2 2) orientation disappeared at 328 K.

Acknowledgements

This work was supported financially by National Natural Science Foundation of China (No. 20776140), National Science Fund for Distinguished Young Scholars of China (No. 20625618) and National 863 Program of China (No. 2006AA06Z317 and No. 2006AA06Z371).

References

[1] D.Q. Wang, Z.Y. Shi, L.J. Zou, Appl. Surf. Sci. 214 (2003) 304.
[2] D.Q. Wang, Z.Y. Shi, Appl. Surf. Sci. 227 (2004) 255.
[3] R.S.C. Paredes, S.C. Amico, A.S.C.M. d'Oliveira, Surf. Coat. Technol. 200 (2006) 3049.
[4] A. Boogard, J.J. van den Broek, Thin Solid Films 401 (2001) 1.
[5] H. Kersten, G.M.W. Kroesen, R. Hippler, Thin Solid Films 332 (1998) 282.
[6] C. Charrier, P. Jacquot, E. Denisse, J.P. Millet, H. Mazille, Surf. Coat. Technol. 90 (1997) 29.
[7] D. Yang, R. Jonnalagadda, B.R. Rogers, J.T. Hillman, R.F. Foster, T.S. Cale, Thin Solid Films 332 (1998) 312.
[8] K. Ziegler, H. Lehmkuhl, Z. Anorg, Allg. Chem. 283 (1956) 414.
[9] E. Peled, E. Gileadi, Plat. Surf. Finish. 62 (1975) 342.
[10] L. Legrand, A. Tranchant, R. Messina, Electrochim. Acta 39 (1994) 1427.
[11] T. Jiang, M.J. Chollier Brym, G. Dube, A. Lasia, G.M. Brisard, Surf. Coat. Technol. 201 (2007) 6309.
[12] D.E. Couch, A. Brenner, J. Electrochem. Soc. 99 (1952) 234.
[13] M. Yoshio, N. Ishibashi, J. Appl. Electrochem. 3 (1973) 321.
[14] M. Yoshio, Met. Finish. 85 (1987) 33.
[15] W. Altgeld, Metalloberfläche 40 (1986) 253.
[16] N. Godshall, J. Electrochem. Soc. 123 (1976) 137C.
[17] J.C. Li, S.H. Nan, Q. Jiang, Surf. Coat. Technol. 106 (1998) 135.
[18] M. Jafarian, M.G. Mahjani, F. Gobal, I. Danaee, J. Appl. Electrochem. 36 (2006) 1169.
[19] B.J. Welch, R.A. Osteryoung, J. Electroanal. Chem. 118 (1981) 455.
[20] P.K. Lai, M.S. Kazacos, J. Electroanal. Chem. 248 (1988) 431.
[21] R.T. Carlin, W. Crawford, M. Bersch, J. Electrochem. Soc. 139 (1992) 2720.
[22] C.C. Yang, Mater. Chem. Phys. 37 (1994) 355.
[23] Y.G. Zhao, T.J. VanderNoot, Electrochim. Acta 42 (1997) 1639.
[24] A.P. Abbott, C.A. Eardley, N.R.S. Farley, A. Pratt, Trans. Inst. Met. Finish. 77 (1999) 26.

[25] T. Tsuda, C.L. Hussey, G.R. Stafford, J. Electrochem. Soc. 151 (2004) C379.
[26] T. Jiang, M.J.C. Brym, G. Dube, A. Lasia, G.M. Brisard, Surf. Coat. Technol. 201 (2006) 1.
[27] J.S. Wilkes, J.A. Levisky, R.A. Wilson, C.L. Hussey, Inorg. Chem. 21 (1982) 1263.
[28] R.T. Carlin, R.A. Osteryoung, J. Electrochem. Soc. 136 (1989) 1409.
[29] A.P. Abbott, C.A. Eardley, N.R.S. Farley, G.A. Griffith, A. Pratt, J. Appl. Electrochem. 31 (2001) 1345.
[30] J.J. Lee, I.T. Bae, D.A. Scherson, B. Miller, K.A. Wheeler, J. Electrochem. Soc. 147 (2000) 562.
[31] C.A. Zell, F. Endres, W. Freyland, Phys. Chem. Chem. Phys. 1 (1999) 694.
[32] Q. Liao, W.R. Pitner, G. Stewart, C.L. Hussey, G.R. Stafford, J. Electrochem. Soc. 144 (1997) 936.
[33] V. Kamavaram, D. Mantha, R.G. Reddy, Electrochim. Acta 50 (2005) 3286.
[34] Q.X. Liu, S. Zein El Abedin, F. Endres, Surf. Coat. Technol. 201 (2006) 1352.
[35] N.A. Pangarov, J. Electroanal. Chem. 9 (1965) 70.
[36] G.B. Harris, Philos. Mag. 43 (1952) 113.
[37] Y. Kato, M. Tatano, S. Takahashi, Nisshin Seikou Gihou 61 (1989) 44.
[38] T. Tsuda, T. Nohira, Y. Ito, Electrochim. Acta 47 (2002) 2817.